nature portfolio

Peer Review File

Multi-omic lineage tracing predicts the transcriptional, epigenetic and genetic determinants of cancer evolution

Reviewers' Comments:

Reviewer #1:
Remarks to the Author:
The manuscript by Nadalin et al uses cutting edge technology to investigate genetic, epigenetic and transcriptional elements that are linked to cancer evolution in the SUM 159 cell line. They correlate tumor initiation in vivo with individual barcoded cells and their transcriptional state, and also examine drug tolerance in relation to transcriptional states. The authors show that clones with tumor-initiating capacity display two transcriptional states at baseline and that these share chromatin accessible regulons, suggesting that pre-existing epigenetic states can determine tumor initiation. The drug tolerant clones shared some overlap with the tumor-initiating state, but two distinct lineages and trajectories were seen to be associated with drug tolerance. The experiments to correlate end-point with initial gene expression data are well-designed, and the data throughout are well described and interesting. The main novelty in this study lies in the application of cutting-edge technology: single cell, multi-omic analysis and tracing of cells through tumor development and drug treatment both in vivo and in vitro.

The main concern is that the whole study is based on one cell line, SUM 159PT, which the authors acknowledge is intrinsically heterogeneous. It belongs to the claudin-low mesenchymal subtype and therefore is atypical of TNBC. It is important to determine whether the tumor initiation S1/S3 signatures or the pathways to drug tolerance can be recapitulated in another TNBC cell line or PDX model. The findings may be unique to this cell line and not clinically relevant. Do the S1 and S3 signatures apply to another cell line/PDX model in vitro (or in vivo)? Moreover, the authors state in Discussion that the amplification on chr 11 has not been reported previously as a recurrent amplicon in cancer (nor breast cancer subtypes), suggesting this locus is not a genetic driver.

Other points:

-In Fig 1B, the number of clones increase on passaging (eg from 3200 to close to 4500) in both experiments – the reverse would have been expected.

-The transplant experiment of Fig 2G would normally compare the TM4SF1hi population against the TM4SF1lo population rather than versus bulk cells (which is assumed to mean everything, but it is not clear). Furthermore, Fig S4 says the transplanted cells come from frozen vials that have been cultured for 9 days. The rationale for not using fresh cells after the sort is unclear since they will change during the 9 day culture period.

-In the analysis of Pal et al data (Fig S3), most of the cells appear to come from one patient, 125 (or cannot be seen for two of the tumors?), therefore it is difficult to know how the "shared' box is defined. The S1, S2 and S3 signatures are also spread through the remaining clusters, so the conclusions/interpretation are not clear.

-The effect of paclitaxel in vivo was very modest, did the authors attempt a higher dose to achieve a drug tolerant state? However, it was useful to perform two rounds of treatment
to examine the drug resistant state. The question relates to the drug tolerant state in a system where the drug effect is very mild.

-In the introduction (second para), there are a few groups that have used clonal barcoding specific to breast cancer (tumor growth and metastasis) which should be included such as Nguyen Nat Commun 2014; Echeverria et al Nat Commun 2018; Merino et al Nat Commun 2019.

Reviewer #2:

Remarks to the Author:
NCOMMS-23-37026-T
The proposed manuscript by Nadalin et al. aims to disentangle genetic, epigenetic and transcriptional determinants of drug tolerance and tumor initiation by employing a combination of state-of-the-art lineage tracing (cellular barcoding), single-cell multiomic and phenotypic assays to a breast cancer model (TNBC, SUM159PT). Utilizing the SUM159PT model, both in vitro and in vivo, they identify three transcriptionally stable clusters via scRNAseq. Tumor initiating clones (TIC) and Drug tolerant clones (DTC) seem to be enriched for distinct transcriptional states pre-existing already at baseline. Notably, the authors identify TM4SF1 as a surface marker for the S1-TIC transcriptomic state and subsequent FAC-sorting for TM4SF1 converges with higher tumor initiation efficiency, as shown by dilution-implantation assays. On the other hand, cluster S3 displayed resistance to paclitaxel chemotherapy in both in vitro and in vivo setups. By leveraging GALILEO, a platform that combines single-cell multiome ATAC with gene expression sequencing, the team discerned distinct modules that aligned with transcriptional profiles and correlated with TIC/DTC status. A notable finding was the identification of a chromosomal amplification on chromosome 11 in the S3 cluster, leading to a DTC phenotype.

Overall, this study is undeniably innovative, showcasing rigorous conduct and robust analyses. The authors show elegantly that tumor evolution can be driven by a mixture of transcriptional, epigenetic and genetic events.

However, the primary limitation is its reliance on a singular model, SUM159PT, which raises concerns regarding generalizability. While the authors did attempt to corroborate their findings using external publications, broader validation is warranted to fortify their conclusions.

General comment: It is unusual not to find summarizing titles for each main figure.

While the study's strengths are evident, there are a few aspects that merit further attention and clarification.

- Figure 1D and corresponding silhouette plots in Figure S1E should be harmonized regarding cluster numbering (UMAP cluster 1-7, Silhouette cluster 0-6). The majority of S3-cluster-cells at T1 exhibit negative silhouette scores, indicative of “misclustering”, could you comment on that? How would the ROGUE entropy measure score here?

- As the UMAP space of Figure 1D T0 serves as “orientation” regarding the TIC and DTC overlay with S1,2,3 and remaining clusters in Figure 2 and 3, it would be informative to investigate “dynamic” relationships of all 7 transcriptional clusters using pseudotime and/or RNA velocity analyses.

- Figure 2C. Could you comment on the overall lower relative clone count of tumor 3?

- How many clones are shared among all 9 tumors? Of S1 or S3 identity?

- As mentioned above, the predominant reliance on the SUM159PT model, while methodologically consistent, potentially limits the generalizability of the findings. Although the authors mapped some S1 and S3 signatures onto external TNBC and PDAC datasets, a broader validation across multiple clinical datasets or alternate models is essential. This would solidify the signatures' roles in tumor initiation and drug resistance. Leveraging publicly available data for this validation would be acceptable. Similar studies performed in melanoma by Arjun Raj’s group could be a valuable source for cross-validation and discussion (PMID: 28607484 PMID: 37468627).

- While sorting for TM4SF1 seems to enrich for faster and more efficient tumor initiation, sorting for a single marker is risky. Having the “ABCB5+ tumor initiating marker” debate from 2010 in mind, I would have appreciated to see FACS-enrichment for TIC-capacity by more than one marker.

- Even though S2 seems to be a transcriptionally distinct and stable (recurrent) cluster/state it seems to be unrelated with either tumor initiation or drug tolerance. That’s surprising as REACTOME enrichment terms include “response to starvation” and many terms related to translation, all known to play roles in drug responses. Any explanation/speculation?

- The employment of an inducible CRISPR interference strategy targeting regions proximal to COL6A1 and COL6A2, which are notably accessible in S1 cells, led to a reduction in COL6A1 and COL6A2 expression. How does this alteration impact tumor initiation and drug resistance capacities on the SUM159PT model?

- Although the study is rich in advanced analytical techniques, its complexity may serve as a barrier to readers who are not well-versed in these specific methods. To enhance reader comprehension, the authors should consider providing concise explanations of specialized analytical techniques used. For instance, in the section "GALILEO links cancer clones with transcriptional programs and DNA accessibility states at single-cell resolution", a brief, one-sentence summary of the referenced method (Bravo Gonzalez-Blas et al. 2019) could facilitate a more accessible understanding without necessitating a separate literature review.

We thank the reviewers for their positive feedback and insightful comments.

For the sake of clarity, we report below the changes we made to the order of the **Supplementary Figures**:

S1 old >> S1 new
S2 old >> S4 new
S3 old >> S3 new
S4 old >> S5 new
S5 old >> S6 new
S6 old >> S7 new
S7 old >> S8 new
S8 old >> S9 new
S9 old >> S10 new
S10 old >> S11new
S11 old >> S12 new
S12 old >> S13 new
S2 new is a new figure

Also, in response to Reviewer 2's general comment, we added a summarising title to each figure.

From the **original** manuscript we removed the following references:

1. Fu, F., et al. (2020). "Role of Transmembrane 4 L Six Family 1 in the Development and Progression of Cancer." Front Mol Biosci **7**: 202.
2. Zukauskas, A., et al. (2011). "TM4SF1: a tetraspanin-like protein necessary for nanopodia formation and endothelial cell migration." Angiogenesis **14**(3): 345-354

In the **revised** manuscript, we added:

1. Echeverria GV*, et al.* High-resolution clonal mapping of multi-organ metastasis in triple negative breast cancer. *Nat Commun* **9**, 5079 (2018).
2. Merino D*, et al.* Barcoding reveals complex clonal behavior in patient-derived xenografts of metastatic triple negative breast cancer. *Nat Commun* **10**, 766 (2019).
3. Nguyen LV*, et al.* DNA barcoding reveals diverse growth kinetics of human breast tumour subclones in serially passaged xenografts. *Nat Commun* **5**, 5871 (2014).
4. Ferrari E, Gandellini P. Unveiling the ups and downs of miR-205 in physiology and cancer: transcriptional and post-transcriptional mechanisms. *Cell Death Dis* **11**, 980 (2020).
5. Mendez O*, et al.* Extracellular HMGA1 Promotes Tumor Invasion and Metastasis in Triple-Negative Breast Cancer. *Clin Cancer Res* **24**, 6367-6382 (2018).
6. Curtis C*, et al.* The genomic and transcriptomic architecture of 2,000 breast tumours reveals novel subgroups. *Nature* **486**, 346-352 (2012).
7. Cancer Genome Atlas N. Comprehensive molecular portraits of human breast tumours. *Nature* **490**, 61-70 (2012).
8. Gavish A*, et al.* Hallmarks of transcriptional intratumour heterogeneity across a thousand tumours. *Nature* **618**, 598-606 (2023).
9. Chen G*, et al.* Targeting TM4SF1 exhibits therapeutic potential via inhibition of cancer stem cells. *Signal Transduct Target Ther* **7**, 350 (2022).
10. Gao H*, et al.* Multi-organ Site Metastatic Reactivation Mediated by Non-canonical Discoidin Domain Receptor 1 Signaling. *Cell* **166**, 47-62 (2016).
11. Pece S*, et al.* Biological and molecular heterogeneity of breast cancers correlates with their cancer stem cell content. *Cell* **140**, 62-73 (2010).
12. Liu B, Li C, Li Z, Wang D, Ren X, Zhang Z. An entropy-based metric for assessing the purity of single cell populations. *Nat Commun* **11**, 3155 (2020).

All the other changes are referred to in greater detail **at the end of each response**.

REVIEWER COMMENTS

Reviewer #1 (Remarks to the Author):

The manuscript by Nadalin et al uses cutting edge technology to investigate genetic, epigenetic and transcriptional elements that are linked to cancer evolution in the SUM 159 cell line. They correlate tumor initiation in vivo with individual barcoded cells and their transcriptional state, and also examine drug tolerance in relation to transcriptional states. The authors show that clones with tumor-initiating capacity display two transcriptional states at baseline and that these share chromatin accessible regulons, suggesting that pre-existing epigenetic states can determine tumor initiation. The drug tolerant clones shared some overlap with the tumor-initiating state, but two distinct lineages and trajectories were seen to be associated with drug tolerance.

The experiments to correlate end-point with initial gene expression data are well-designed, and the data throughout are well described and interesting. The main novelty in this study lies in the application of cutting-edge technology: single cell, multi-omic analysis and tracing of cells through tumor development and drug treatment both in vivo and in vitro.

Reviewer1.Q1. *The main concern is that the whole study is based on one cell line, SUM159PT, which the authors acknowledge is intrinsically heterogeneous. It belongs to the claudin-low mesenchymal subtype and therefore is atypical of TNBC. It is important to determine whether the tumor initiation S1/S3 signatures or the pathways to drug tolerance can be recapitulated in another TNBC cell line or PDX model. The findings may be unique to this cell line and not clinically relevant. Do the S1 and S3 signatures apply to another cell line/PDX model in vitro (or in vivo)? Moreover, the authors state in Discussion that the amplification on chr 11 has not been reported previously as a recurrent amplicon in cancer (nor breast cancer subtypes), suggesting this locus is not a genetic driver.*

Reviewer1.R1. We appreciate the reviewer's insightful comment and recognize the importance of extending our findings to a broader breast cancer context. Below, we address the following points: (**1)** relevance of SUM159PT as a TNBC model; **(2)** generalisability of S1, S2 and S3 gene signatures; and **(3)** recurrence of chr11:118M-126M amplification in breast cancer. We further expand this point in **Reviewer2.R5**, where we show the generalisability to primary tumour dataset in great detail and provide further methodological descriptions and details.

(1) relevance of SUM159PT as a TNBC model. To assess the relevance of SUM159PT transcriptional programs in primary TNBC tumours, we leveraged the substantial amount of molecular information provided by the Molecular Taxonomy of Breast Cancer International Consortium (METABRIC (DOI: 10.1038/nature10983)) and The Cancer Genome Atlas (TCGA (DOI: 10.1038/nature11412). Specifically, we explored the gene expression distribution of the S1, S2 and S3 signatures across breast cancer subtypes. At the individual gene level, we observed that i) most of the genes of each signature are expressed in primary breast tumours, even outside the claudin low subtype and ii) clustering by correlation identifies at least two main groups of co-expressed genes, suggesting that they might be part of the same network even in “real” tumours (see **Reviewer2.R5**). For each gene signature and for each dataset, we first define two thresholds, separating samples into high, medium, and low aggregate expression of the signature (see Methods for details). Below we report the stratification of breast cancer tumours according to high, medium, and low S1, S2 and S3 aggregate gene expression, respectively, in all TCGA and METABRIC breast cancer datasets.

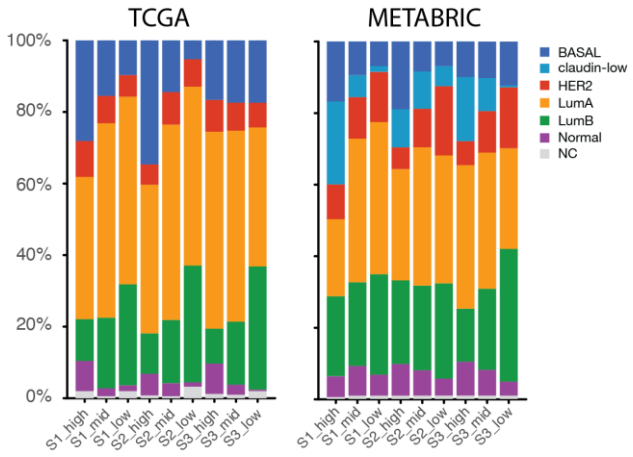

Figure R1.1. Stratification of breast cancer samples into the breast molecular subtypes according to subpopulation signatures' activity (see Methods) in TCGA (left) and METABRIC (right) datasets. NC, not classified.

Our analysis revealed that S1 and S2 signatures were associated to the basal tumours subtype in both TCGA e METABRIC datasets, while S1 and S3 signature were also associated to the claudin low subtype (which accounts for 9.8% of all tumours in METABRIC). Basal and Claudin-low subtypes are both strongly enriched for TNBC tumours (Cancer Genome Atlas) suggesting that our signatures are not capturing merely a feature of Claudin-low cells.

(2) generalisability of S1, S2, S3 gene signatures. We performed scRNA-Seq sequencing on the TNBC cell line MDA-MB-231 TGL (referred to as MDA-MB-231 below) and obtained 4610 high-quality gene expression profiles, which grouped into 7 clusters, shown on UMAP below (the analysis was performed in a similar way as for SUM159PT cells).

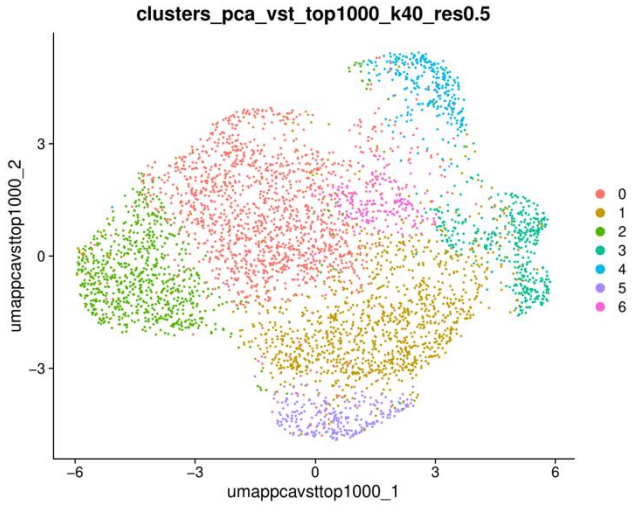

Figure R1.2. UMAP representation of MDA-MB-231 TGL (4610 cells) coloured by cluster.

The transcriptional landscape of cancer cell lines is known to be heterogeneous, notably in breast (Gambardella et al. (DOI: 10.1038/s41467-022-29358-6). To find shared transcriptional programs between SUM159PT and MDA-MB-231, we first quantified signature gene expression in the MDA-MB-231 clusters. We note that S1 is the most transcriptionally distinguishable SUM159PT subpopulation, whereas S2 and S3 show only subtle gene expression differences compared to the other SUM159PT cells, and, therefore, are more difficult to identify. S1 harbour over 100 differentially expressed genes, both at T0 and T1, relative to all the other cells, therefore we focus on the recurrence of S1 signature genes in MDA-MB-231 (below we provide extensive evidence for the functional relevance of the S1 signature in cancer). Below are violin plots showing the log-normalized gene expression values of some

among the top 20 significant S1 genes; these are not randomly distributed across clusters, but are higher in cluster 4 and, secondarily, in cluster 3, hinting that the transcriptional profile of S1 may be recurrent in specific MDA-MB-231 cell subpopulations.

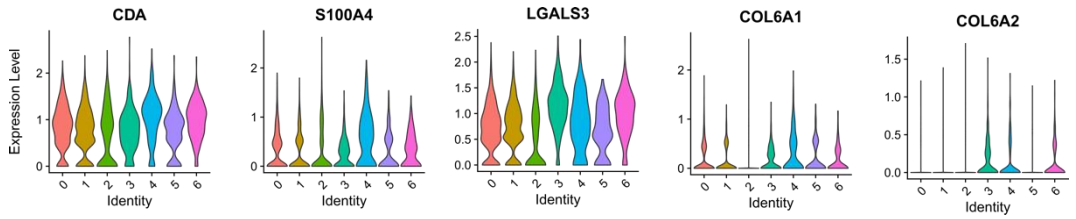

Figure R1.3. Violin plots showing the log-normalised expression of selected S1 signature genes across MDA-MB-231 TGL clusters.

Then, we asked whether SUM159PT and MDA-MB-231 heterogeneity can recapitulate the gene expression programs found in primary tumours. To this aim, we considered the Curated Cancer Cell Atlas (3CA, https://www.weizmann.ac.il/sites/3CA/), which contains single-cell transcriptional profiles for primary tumours, for many cancer types (see **R2.Q5** as it provides full methodological descriptions of the analysis and details of the SUM159PT results). This resource comes with a set of gene meta-programs, whose expression is heterogeneous within a single tumour; some of these meta-programs are also recurrent across cancer types. Therefore, we computed the joint expression of meta-programs in SUM159PT and MDA-MB-231 cells and related it with cell clusters (see **R2.Q5** for a detailed description of the analysis). This comparison allows us to assess whether the transcriptional heterogeneity of the two cancer cell lines is representative of TNBC (and more generally of cancer) heterogeneity. The heatmaps below show the association (AUC) between meta-programs expression (only meta-programs shared across multiple tumours shown) and SUM159PT and MDA-MB-231 clusters, respectively.

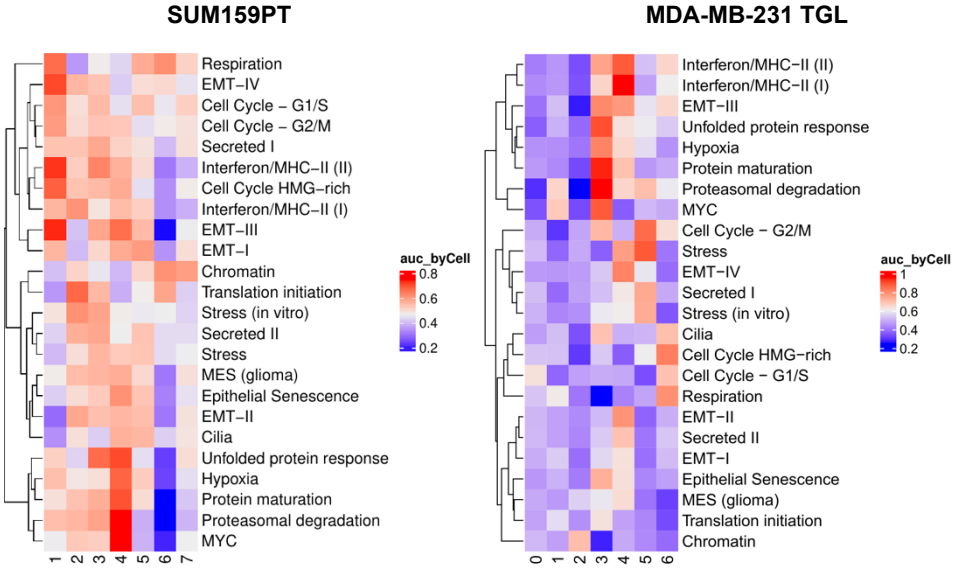

Figure R1.4. Association of gene meta-programs from [Gavish, 2023] with SUM159PT (left) and MDA-MB-231 TGL (right) clusters. Only "shared" meta-programs are reported. The entries are the AUC values where the predictor is the aggregate meta-program expression, and the response is the membership to each cluster.

Meta-program expression varies across clusters (SUM159PT inter-cluster AUC correlation: mean = -0.14, st. dev. = 0.38) and is recurrent across the two models: for instance, we observe a strong association between cluster 1 (S1) in SUM159PT and cluster 3-4 in MDA-MB-231 with the “EMT-III” and “Interferon/MHC-II (II)” meta-programs, respectively, suggesting again a correspondence between

SUM159PT and MDA-MB-231 cells. Below we report a more detailed view of the associations of MDA-MB-231 clusters with meta-programs (SUM159PT gene signatures are labelled; see **Reviewer2.R5** for the association of meta-programs to SUM159PT clusters).

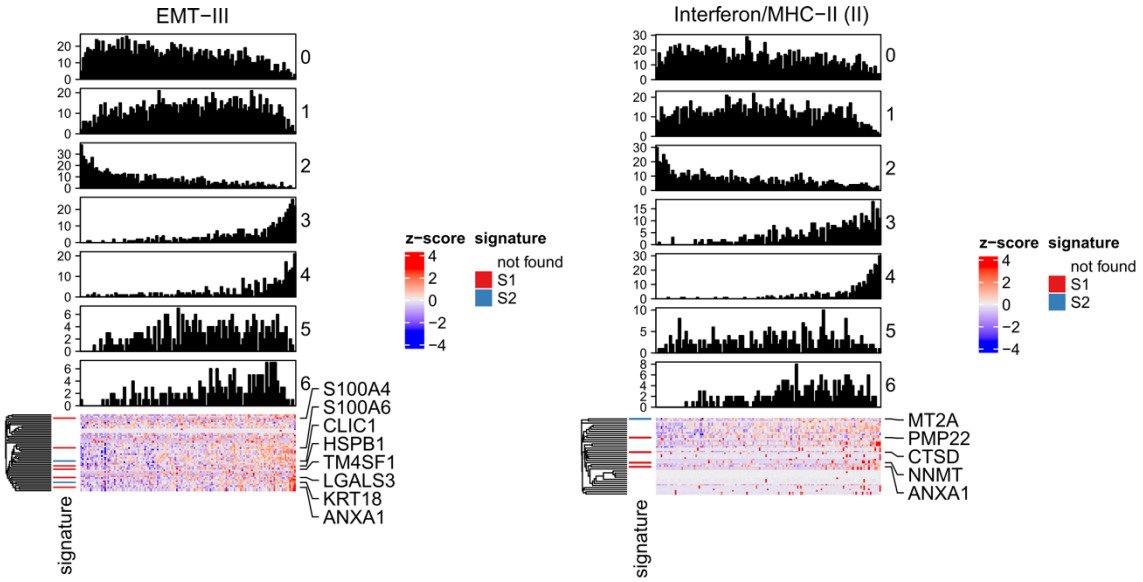

Figure R1.6. Detailed association of two meta-programs with MDA-MB-231 TGL clusters. The columns of the heatmaps represent the cells ordered by non-decreasing meta-program expression; the genes common to the subpopulation signatures are marked in color and labelled. The bar plots show the binned cell count (100 bins) for each subpopulation.

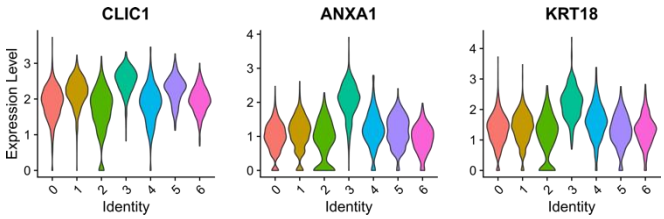

Figure R1.7. Violin plots showing the log-normalised expression of selected genes in the meta-program across MDA-MB-231 TGL clusters.

MDA-MB-231 cluster 3 cells show high expression of S1 markers, notably CLIC1, ANXA1 and KRT18, which are among the top 50 significant genes for the “EMT-III” meta-program (see violin plots).

The parallelism with the MDA-MB-231 and the overall generalizability of our results is further supported by the evidence indicating that TM4SF1, one of the primary markers of S1 that we used for isolating sub-populations enriched in tumour-initiating cells, is also identified in other cancer models. Notably, TM4SF1 enrichment correlates precisely with tumour-initiating capacity, as observed in human MDA-MB-231 cells, murine 4T1 breast cancer cells, and MMTV-Neu tumours (Gao et al. (DOI: 10.1016/j.cell.2016.06.009); Chen et al. (DOI: 10.1038/s41392-022-01177-7)).

Taken together, these results suggest that SUM159PT gene signatures are both generalisable and clinically relevant.

Finally, we clarify below the enrichment of S1, S2, and S3 signatures we obtained with Scissor (see Methods) in the breast cancer scRNA-Seq dataset from Pal *et al.* (DOI: 10.15252/embj.2020107333) (see **Figure S3**). We obtained 9 scRNA-Seq clusters on the primary tumour samples and computed the

odds-ratio for each signature-cluster pair. The result of the calculation is reported below (odds-ratio > 1 means positive enrichment).

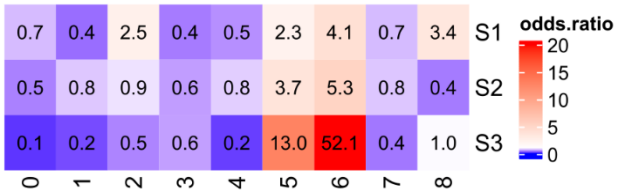

Figure R1.8. Odds-ratio comparing the fraction of cells in each cluster-phenotype pair for [Pal 2021] dataset; clusters (in columns) and phenotype-positive cell subsets (in rows) as in **Suppl. Figure 3B.**

Cluster 6 contains cells from all 4 donors (see also **Reviewer1.R4.**) and shows the highest enrichment for each subpopulation, suggesting that transcriptionally stable SUM159PT clones match cells of cluster 6 in primary breast tumours. We note, however, that cluster 5 is overall enriched in signature-labelled cells (odds-ratio > 1 for S1, S2 and S3). Cluster 5 only contains cells from sample 126, which suggests that this specific patient shows high transcriptional similarity with the SUM159PT model.

We added two new panels in **Figure 1 (H** and **I)**, a new **Suppl. Figure 2**, a new panel in **Suppl. Figure 3 (C)** and two **Suppl. Tables 5 and 6**. We added a new paragraph entitled "**SUM159PT transcriptional heterogeneity is recapitulated in primary tumours**" and moved there the description of the analysis of the dataset from Pal et al., which was previously included in "The baseline programs S1 and S3 predict tumour initiation".

3) recurrence of chr11:118M-126M amplification in breast cancer. We tested whether this specific genetic alteration is also found in patients, leveraging the TCGA breast cancer dataset (GISTIC tool, cBioPortal). We searched for samples bearing a copy-number gain on the 237 genes spanned by the amplicon. This analysis highlighted a small subset of tumours (73 out of 1084), primarily within the basal type (30%; q-value 9.735e-4, Chi-Squared test with Benjamini-Hochberg correction), with a copy-number gain across all the 237 genes. However, the amplified region extended to a larger fraction of the 11q arm (see **Figure R1.9 below**). Furthermore, TCGA contains pre-treatment samples, where we expect a lower copy-number gain compared to a post-treatment condition. Therefore, we could confirm the existence of amplification in breast cancer and basal tumours spanning the chr11:118M-126M region. However, we could not assess whether this event is associated with resistance to chemotherapy treatments. Noteworthy, among the 24 genes lying this region is MIR100HG, a long non-coding RNA (lncRNA) precursor of two microRNAs, miR-100 and miR-125b. These microRNAs have been demonstrated to mediate resistance to drug treatments, including paclitaxel, in various tumour types (as indicated by Zhou et al. (DOI: 10.1074/jbc.M109.083337); Lu et al. (DOI: 10.1038/nm.4424) mentioned in the Discussion).

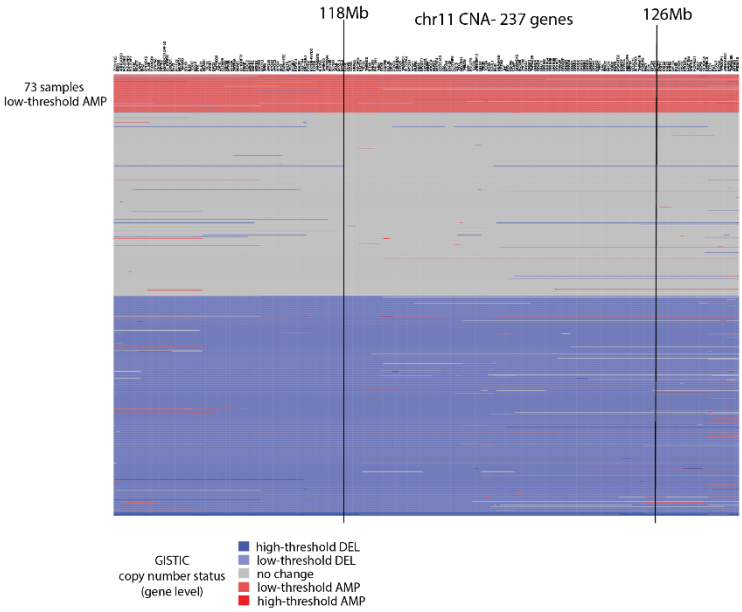

Figure R1.9. GISTIC-based copy number status of the genes belonging to the chr11:118M-126M amplification and nearby regions in the TCGA breast cancer cohort. Shown are predicted deletions (DEL) and amplifications (AMP) at two confidence levels; high-level thresholds are calculated on a sample-by-sample basis and are based on the maximum (or minimum) median arm-level amplification (or deletion) copy number found in the sample. Here most genes satisfy only low-level thresholds, implying that the copy number alteration extends to a wider chr11 region.

Other points:

Reviewer1.Q2. *In Fig 1B, the number of clones increase on passaging (eg from 3200 to close to 4500) in both experiments – the reverse would have been expected.*

Reviewer1.R2. We thank the reviewer for this comment. A greater number of clones collected at T1 is due to the number of cells retained, which ultimately depends on the scRNA-Seq experiment design – namely, the cell recovery for a single replicate was below 10000 cells for any replicate (see the table below), therefore we could only sample a subset of the > 10000 GBC species in each scRNA-Seq experiment. After removing low quality cells, doublets and cells expressing 0 GBCs (see Methods, “Quality filtering and normalisation”), we obtained 10038 and 14265 cells for T0 and T1, respectively (over two replicates per time point; these counts differ from the one reported in **Figure 1D**, because a second filtering step was applied there to remove small, low-quality clusters; see Methods, “Dimensional reduction and clustering”). Among these cells, we detected 6484 and 8670 unique clones in T0 and T1, respectively. These cell and clone counts correspond to the bar plots of **Suppl. Figure 1A** and are reported in the table below. The number of cells per clone in T0 and T1 samples is similar, highlighting that passaging has no effect on clone selection.

sample	clone.count	cell.count	cells.per.clone
T0_1	3816	6239	1.63
T0_2	2668	3799	1.42
T1_1	4419	7395	1.67
T1_2	4251	6870	1.62

Table R1.1. Sc-RNA-Seq sample statistic (parental, untreated; T0 and T1). The number of clones is the number of unique GBC sets expressed in a single cell.

Reviewer1.Q3. *The transplant experiment of Fig 2G would normally compare the TM4SF1hi population against the TM4SF1lo population rather than versus bulk cells (which is assumed to mean everything, but it is not clear). Furthermore, Fig S4 says the transplanted cells come from frozen vials that have been cultured for 9 days. The rationale for not using fresh cells after the sort is unclear since they will change during the 9 day culture period.*

Reviewer1.R3. The three main goals of this experiment were: 1) assessing the increased ability of the S1 subpopulation, as compared to the bulk SUM159PT population, to initiate tumours *in vivo*; 2) providing a fine-grained characterisation of the S1 population at the gene expression level, and 3) performing CRISPRi experiments on isolated S1 cells.

We employed vials frozen at 9 days (D9) for the following reasons. Sorting is known to induce stress on cells; indeed, we noticed that freshly sorted cells showed activation of some stress and inflammatory pathways (*e.g.*, the STAT1 regulon, see the new **Suppl. Figure 6D, previously Suppl. Figure 5D**). **Figure 2G** shows the gene expression profile of both TM4SF1-high and bulk cells over passages: the expression of most S1 signature genes (marked in red) in TM4SF1-high cells is stable at day 9 (D9) (including relevant EMT-III markers discussed in **Reviewer1.R1** above, *e.g.,* TM4SF1, S100A4 and LGALS3; see **Suppl. Figure 6A-C, previously Suppl. Figure 5A-C,** and **Suppl. Table 9**). Conversely, we observed that a pool of genes associated to stress response, but not belonging to the S1 signature, is upregulated in the freshly sorted population, but is lost at D9. Therefore, we used the cells at D9 for both the *in vivo* and CRISPRi functional experiments shown in **Figure 4**. Importantly, before *in vivo* transplant, the expression of key markers on isolated cells was measured by RT-qPCR (**Suppl. Figure 6A, previously Suppl. Figure 5A**).

The transplant experiment was performed using the TM4SF1-high fraction against the entire SUM159PT population ('bulk'; in this case, cells were FAC-sorted to account for biases, as described above, but no gating was applied). In agreement with aim 1) above, we sought to employ the bulk population rather than TM4SF1-low population. Our objective was to ensure that the TM4SF1-high population contained S1 cells, while minimising the number of TM4SF1-high, non-S1 cells. We did not observe a clear bimodal pattern in the TM4SF1 signal distribution (**Figure 2G**); therefore, we sorted TM4SF1-high cells by setting the gate either at top 5% or top 10% fluorescence (new **Suppl. Figure 5D**) and observed that the expression of key S1 markers (measured by both RT-qPCR and bulk RNA-Seq, **Suppl. Figure 6B, previously Suppl. Figure 5B**) decreased in the top 10% compared to the top 5% population.

We added a new panel in **Suppl. Figure 5, previously Suppl. Figure 4**, showing the TM5SF1 gating strategy.

Reviewer1.Q4. *In the analysis of Pal et al data (Fig S3), most of the cells appear to come from one patient, 125 (or cannot be seen for two of the tumors?), therefore it is difficult to know how the "shared' box is defined. The S1, S2 and S3 signatures are also spread through the remaining clusters, so the conclusions/interpretation are not clear.*

Reviewer1.R4. Patient 125 contains most of the epithelial cells (selected via EPCAM expression; see Methods), as reported in the below table.

sample.id	106	114	125	126
cell.count	40	140	7979	904

Table R1.2. ScRNA-Seq sample statistics from [Pal 2021] (epithelial cells only, selected on the basis of a threshold on EPCAM normalised expression; sample ID as in [Pal 2021]).

We clustered the cells from the four samples combined (see Methods, "Triple-negative breast cancer (TNBC) scRNA-Seq") and obtained 9 clusters. The "shared" box reported in **Suppl. Figure 3B** highlights the cluster with the most heterogeneous sample composition (cluster 6). The UMAP representation of the clusters and their sample composition are reported below.

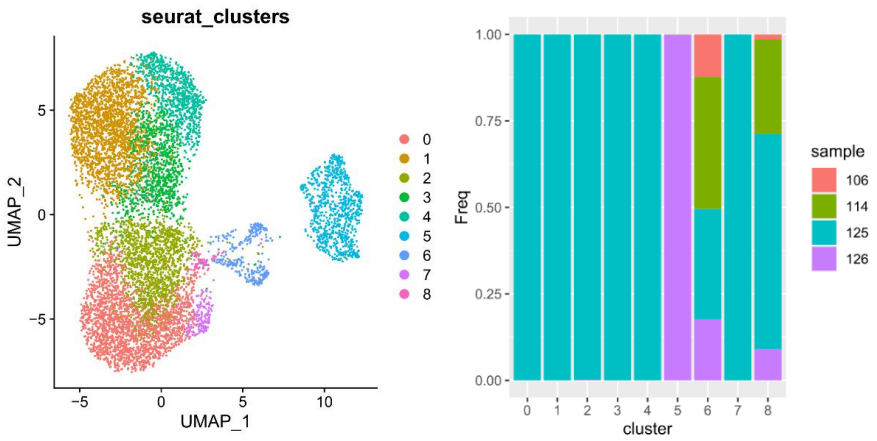

Figure R1.10. ScRNA-Seq clustering for [Pal 2021] dataset. Left: the epithelial (EPCAM⁺) cells from n=4 primary TNBC samples, as in **Table R1.2**, are plotted on gene expression space (UMAP) and coloured by cluster (9063 cells in total). Right: bar plot showing cluster composition.

We added a new panel in **Suppl. Figure 3B** to clarify the cluster composition and the definition of "shared" cluster.

Reviewer1.Q5. *The effect of paclitaxel in vivo was very modest, did the authors attempt a higher dose to achieve a drug tolerant state? However, it was useful to perform two rounds of treatment to examine the drug resistant state. The question relates to the drug tolerant state in a system where the drug effect is very mild.*

Reviewer1.R5. We acknowledge that the effect of Paclitaxel treatment *in vivo* was modest. We conducted all our experimental procedures in compliance with internal and rigorous governmental guidelines. Our authorized protocol (Italian Ministry of Health 779/20) assents the use of a Paclitaxel dose in the range of 10-20 mg/kg. Therefore, we decided to use the no observe adverse effect level (NOAEL) dose that i) would be tolerated and ii) would allow for long-term survival and, therefore, analysis of resistance patterns. Besides, the above dose of is commonly used for short-term studies (Echeverria et al. (DOI: 10.1126/scitranslmed.aav0936); Filippone et al. (DOI: 10.1038/s41467-022-30375-8)).

In vitro, we could employ a more effective dose (50 nM), triggering over 95% cell death (**Suppl. Figure 7A, previously Suppl. Figure 6A**). Such selective conditions allowed us to conclude that, among the three transcriptionally stable subpopulations, only S3 is drug tolerant. Indeed, paclitaxel administration *in vivo*, despite having only minor effect on clone selection, is associated to a diminished expansion of S1 clones and an increased expansion of S3 clones (**Figure 3E**), in agreement with *in vitro* data.

Reviewer1.Q6. *In the introduction (second para), there are a few groups that have used clonal barcoding specific to breast cancer (tumor growth and metastasis) which should be included such as Nguyen Nat Commun 2014; Echeverria et al Nat Commun 2018; Merino et al Nat Commun 2019.*

Reviewer1.R6. We appreciate the reviewer's suggestion, and we have incorporated the recommended references into the revised manuscript.

Reviewer #2 (Remarks to the Author):

The proposed manuscript by Nadalin et al. aims to disentangle genetic, epigenetic and transcriptional determinants of drug tolerance and tumor initiation by employing a combination of state-of-the-art lineage tracing (cellular barcoding), single-cell multiomic and phenotypic assays to a breast cancer model (TNBC, SUM159PT). Utilizing the SUM159PT model, both in vitro and in vivo, they identify three transcriptionally stable clusters via scRNAseq. Tumor initiating clones (TIC) and Drug tolerant clones (DTC) seem to be enriched for distinct transcriptional states pre-existing already at baseline. Notably, the authors identify TM4SF1 as a surface marker for the S1-TIC transcriptomic state and subsequent FAC-sorting for TM4SF1 converges with higher tumor initiation efficiency, as shown by dilution-implantation assays. On the other hand, cluster S3 displayed resistance to paclitaxel chemotherapy in both in vitro and in vivo setups. By leveraging GALILEO, a platform that combines single-cell multiome ATAC with gene expression sequencing, the team discerned distinct modules that aligned with transcriptional profiles and correlated with TIC/DTC status. A notable finding was the identification of a chromosomal amplification on chromosome 11 in the S3 cluster, leading to a DTC phenotype.

Overall, this study is undeniably innovative, showcasing rigorous conduct and robust analyses. The authors show elegantly that tumor evolution can be driven by a mixture of transcriptional, epigenetic and genetic events.

However, the primary limitation is its reliance on a singular model, SUM159PT, which raises concerns regarding generalizability. While the authors did attempt to corroborate their findings using external publications, broader validation is warranted to fortify their conclusions.

General comment: It is unusual not to find summarizing titles for each main figure.

While the study's strengths are evident, there are a few aspects that merit further attention and clarification.

Reviewer2.Q1 *Figure 1D and corresponding silhouette plots in Figure S1E should be harmonized regarding cluster numbering (UMAP cluster 1-7, Silhouette cluster 0-6). The majority of S3-cluster-cells at T1 exhibit negative silhouette scores, indicative of "misclustering", could you comment on that? How would the ROGUE entropy measure score here?*

Reviewer2.R1. Suppl. Figure 1E is now updated, with clusters ordered and coloured as in **Figure 1**.

We computed multiple Louvain clustering runs on the top PCs, whose number was dependent on the choice of the highly variable gene set and determined according to a relative explained standard deviation cut-off, using different values for the number of neighbours in the k-nn graph (k) and clustering resolution (see Methods). We tested r = 0.1 to 0.8 in steps of 0.1 for each parameter set. The top silhouette width solution was found on the 1000 most highly variable genes computed with the vst method (which resulted in top 12 and 15 PCs for T0 and T1, respectively, number of neighbours k = 40, and resolution r = 0.3, for both T0 and T1. Here, our goal was to have a reasonable number of clusters where to compute the clone sharedness score. So, we increased r to 0.5 to detect more clusters.

We thank the reviewer for pointing out an alternative method for measuring the quality of a clustering solution. Silhouette width and ROGUE score capture distinct cluster features: silhouette width assesses the goodness of assignment of a cell c to cluster C compared to the most similar cluster C', by measuring the distance from the clusters' centroids; ROGUE score assesses intra-cluster purity, by computing the gene expression entropy within each cluster. Therefore, silhouette width is high when clusters are very distinct from each other, whether ROGUE is high on homogenous clusters.

We computed ROGUE score on the clustering solutions, using the same set of highly variable genes used to compute PCA and on each replicate separately (n=2). Below, we report silhouette widths and ROGUE scores, for all clusters in T0 and T1 respectively, ordered and coloured as in **Figure 1**.

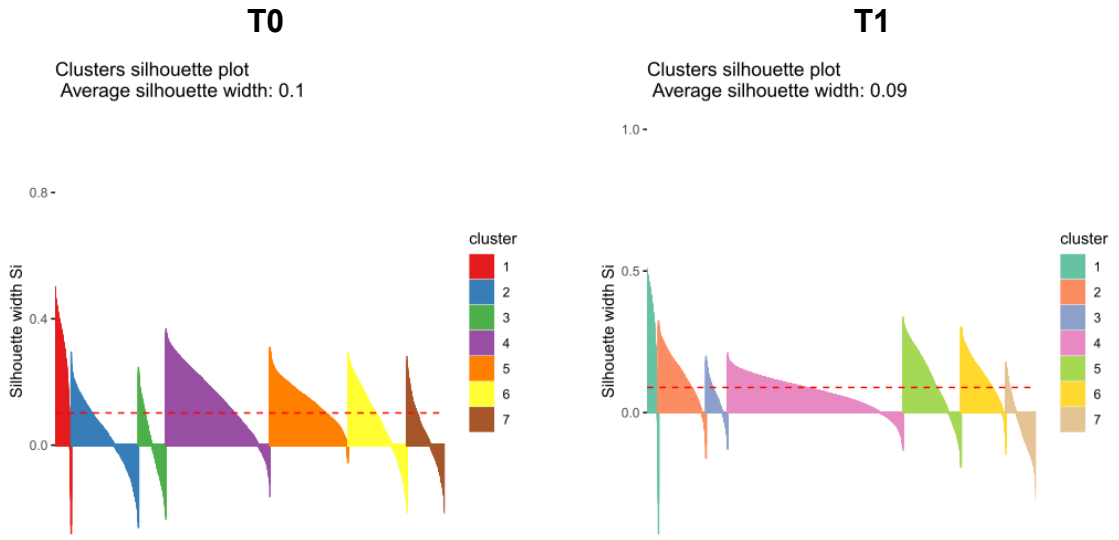

Figure R2.1. Silhouette width for each cell in the selected clustering solutions for T0 (left) and T1 (right) scRNA-Seq SUM159PT samples (n=2 per time point).

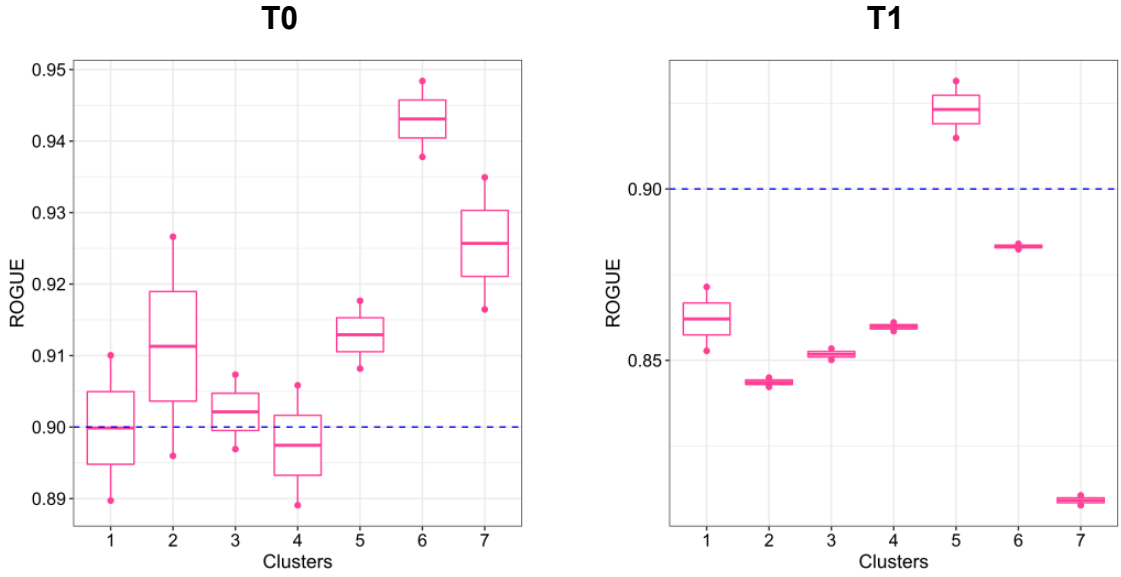

Figure R2.2. ROGUE score for each cell in the selected clustering solutions for T0 (left) and T1 (right) scRNA-Seq SUM159PT samples (n=2 per time point).

The two metrics do not agree with each other on these clustering solutions: for instance, cluster 1, which corresponds to subpopulation S1, shows the highest silhouette width, as its gene expression profile overall is very distinct from that of all the other clusters (see Suppl. Table 2), whereas it shows relatively low ROGUE score, especially at T1, which may suggest that cluster 1 is internally heterogeneous (ROGUE score > 0.9 is indicative of good cluster purity, as per authors' guidelines).

We argue that these two metrics may be used in combination for the selection of clustering solutions representing a good compromise between inter-cluster dissimilarity and intra-cluster homogeneity. Below, we report the average silhouette width and ROGUE score, respectively, across clusters for each resolution value and for the two time points (T0 and T1). Incidentally, resolution 0.5 turns out to be a good compromise between silhouette width and ROGUE score, corroborating the validity of the clustering solution we selected.

We added a new panel in **Suppl. Figure 1** and a new paragraph in Methods, reporting ROGUE scores.

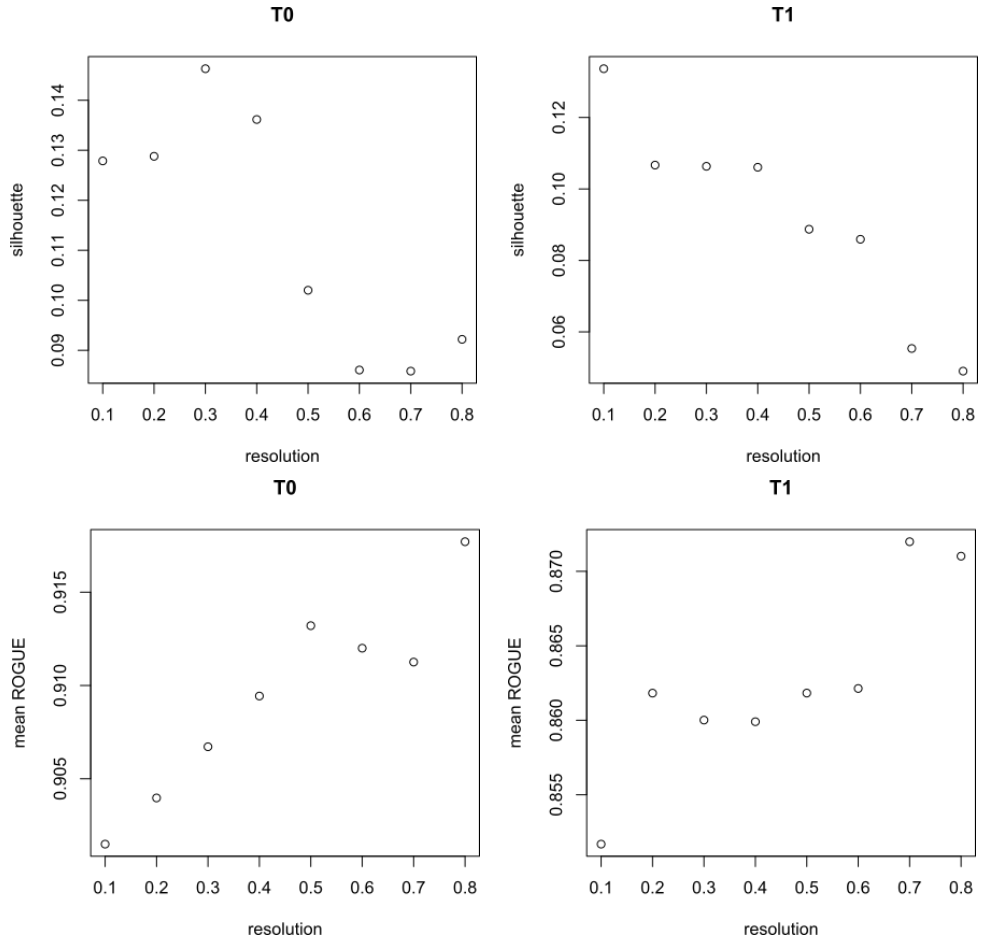

Figure R2.3. Silhouette widths and ROGUE scores for each cell in the SUM159PT clustering solutions generated for each resolution value ranging from r = 0.1 to r = 0.8, for T0 (left) and T1 (right) scRNA-Seq samples (n=2 per time point).

Reviewer2.Q2. *As the UMAP space of Figure 1D T0 serves as "orientation" regarding the TIC and DTC overlay with S1,2,3 and remaining clusters in Figure 2 and 3, it would be informative to investigate "dynamic" relationships of all 7 transcriptional clusters using pseudotime and/or RNA velocity analyses.*

Reviewer2.R2. The advantage of having guide barcodes in our system is that they allow us to directly trace the fate of the cells. In absence of a selective pressure, the three subpopulations S1, S2, S3 are transcriptionally stable: for a cell in S1 at T0, most of its offspring at T1 lie in S1 (likewise for S2 and S3). Additionally, T0 is ahead of T1 by 5-6 cell divisions (see **Figure 1B**) For these reasons, we argue that a tool estimating RNA velocity by capturing cell state transitions using the unspliced / spliced read fraction, which are in the time frame of one cell cycle, cannot capture the relationships among S1, S2 and S3. In contrast, we do not exclude that the clones initially lying in S1, S2 and S3 may undergo major transcriptional changes in a time span longer than 5-6 cell divisions – see, for example, Gupta et al. (DOI: 10.1016/j.cell.2011.07.026) for evidence of human breast cancer cell subpopulations able to stochastically transition across states, ultimately restoring the initial heterogeneity.

Therefore, we considered applying pseudotime inference to link the three subpopulations using transcriptional information. We used the silhouette width for each single cell to evaluate which clusters are more likely to be next to other clusters in a trajectory or rather at the extremities (independently of pseudotime ordering) and select the initial state based on that. Below are reported, for each entry (i,j),

the fraction of cells in cluster i such that the most similar cluster is j according to the cell-cluster centroid distance in PCA space (see **Reviewer2.R1**).

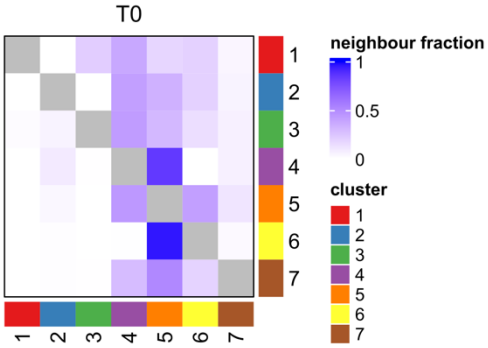

Figure R2.4. Heatmap reporting, for each entry (i,j), the fraction of cells in cluster i such that the most similar cluster is j according to the cell-cluster centroid distance in PCA space (SUM159PT clusters).

Cluster 1 is the closest neighbour for the least number of cells; thus, we label it as the starting point of the trajectory. We applied Slingshot on principal components to infer a trajectory and compute the pseudotime.

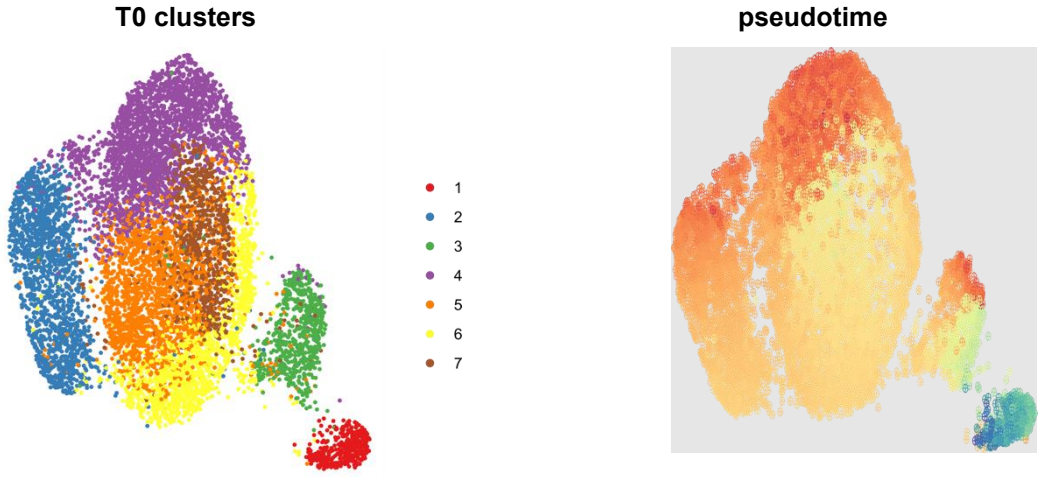

Figure R2.5. UMAP representation of SUM159PT T0 (9395 cells) coloured by cluster (left) or by pseudotime assigned by Slingshot (right).

As shown above, the pseudotime gradient does not order cells according to subpopulations: it only finds that a subset of S3 is close to S1 in pseudotime space. Indeed, S1 and S3 show a partial transcriptional similarity: 9 out of the 29 gene expression markers of S3 are shared with S1, including some of the top ranked in S1 (COL1A1, NPTX2, NREP; see **Figure 1G**); moreover, S1 and S3 share the accessible regions of ATAC Module 1 (see **Figure 4D**).

We thank the reviewer for raising this point, which we now made clearer by adding a sentence in paragraph "**The baseline programs S1 and S3 predict tumour initiation**" to make the partial transcriptional similarity between S1 and S3 more explicit.

Reviewer2.Q3. *Figure 2C. Could you comment on the overall lower relative clone count of tumor 3?*

Reviewer2.R3. We acknowledge the notable difference in clonal abundance between T3 and the other tumours, with T3 containing fewer clones (178 distinct GBCs) compared to the other tumours (1178 GBCs on average). Despite this variability, clonal diversity was not associated with latency in tumour formation. Furthermore, when we assessed clonality using an independent SUM159PT xenograft

cohort, we observed substantial variability, as illustrated in the figure below. Notably, M3D1, M3H1 and M3H3 tumours were predominantly constituted by a single, highly expanding clone (top1, coloured in red). Importantly, the identity of the dominant clone was not recurrent across tumours. Based on these observations, we concluded that the low clonal diversity of T3 is likely stochastic.

We added a sentence in paragraph "**Cancer clones promote tumour initiation in a non-stochastic manner**".

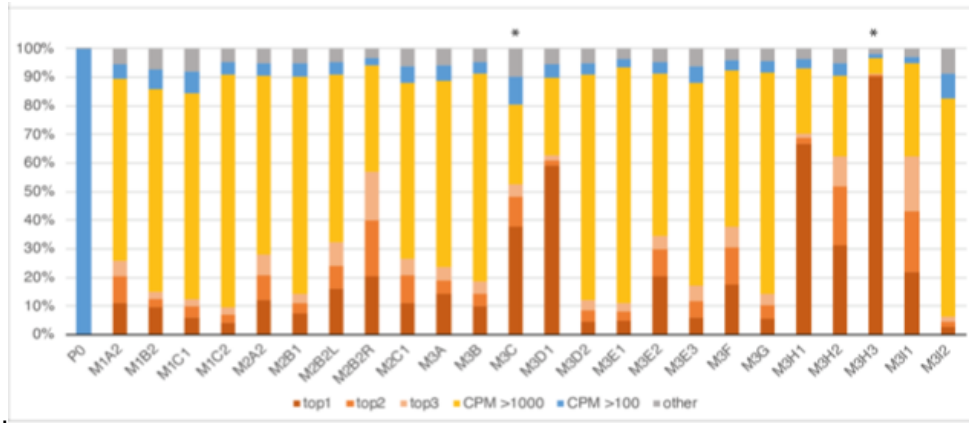

Figure R2.6. Clonality of SUM159PT derived tumours in an independent xenograft cohort. Cells were labelled with a library of ~4000 barcodes and 100K cells injected into each mouse. The stacked bar chart reports the frequency of the top3 barcodes (in % over total copies per million, CPM), as well as the cumulative frequency of those barcodes >1000 or 100 CPM. Note that the library used for this experiment is not the GBC Perturb library used in the present work.

Reviewer2.Q4. *How many clones are shared among all 9 tumors? Of S1 or S3 identity?*

Reviewer2.R4. Figure 2 shows the identification of tumour-initiating clones, which are defined as such based on their ability to **expand** relative to the parental population. Importantly, clone frequency at pre-implantation stage is unrelated to tumour-initiating capacity. Failing to consider this aspect could result in clones with high initial frequencies being more likely to be misclassified as tumour-initiating.

Among the analyzed tumors, **40 clones** are recurrent in all 9 tumours and **127** are recurrent in all 8 non-T3 tumours (see **Reviewer2.R3** and **Suppl. Table 1)**. Notably, 99 out of these 127 clones are classified as TICs according to our strategy, meaning that most of the clones recurrent in all 8 non-T3 tumours are also **expanded** *in vivo* in at least 6 out of 9 tumours compared to the parental population.

We defined TICs based on bulk GBC DNA-Seq, where a clone corresponds to a single GBC. In scRNA-Seq assays, where cell clusters are defined, both single- and co-infections can be detected, and a clone can be associated to one or more GBCs; conversely, a single GBC can be detected in multiple cells and, thus, in multiple clusters. The single-cell cluster labelling is transferred to a bulk sample by selecting only non-ambiguous assignments, as follows: a GBC is associated to cluster *C* if and only if all cells where that GBC is detected belong to cluster *C*, otherwise the GBC is left unclassified (see Methods and **Suppl. Table 1**). We consider the **127** clones (GBCs) recurrent in all 8 non-T3 tumours. Below, we report their frequency in the two scRNA-Seq experiments T0 and T1, both in the whole sample and in each cluster. We note that most of the non-ambiguous GBCs as defined above belong to S1 and S3, consistent with their definition as tumour-initiating subpopulations.

	in all 8 non-T3 tumors		overall		% of the cluster	
	EXP 1B	EXP 1D	EXP 1B	EXP 1D	% 1B	% 1D
S1	15	18	125	125	12,0%	14,4%
S2	1	0	709	542	0,1%	0,0%
S3	51	35	346	316	14,7%	11,1%
CL4	1	1	694	1316	0,1%	0,1%
CL5	0	1	492	203	0,0%	0,5%
CL6	5	1	409	289	1,2%	0,3%
CL7	0	1	201	102	0,0%	1,0%
unclass / not found	54	70	10395	10478	0,5%	0,7%
tot clones	127	127	13371	13371		

Table R2.1. Tumour composition statistics, where only non-ambiguous assignments of bulk GBCs to scRNA-Seq clones are considered.

We added a sentence in paragraph "**Cancer clones promote tumour initiation in a non-stochastic manner**" clarifying the importance of accounting for the initial clone frequency when classifying TICs.

Reviewer2.Q5. *As mentioned above, the predominant reliance on the SUM159PT model, while methodologically consistent, potentially limits the generalizability of the findings. Although the authors mapped some S1 and S3 signatures onto external TNBC and PDAC datasets, a broader validation across multiple clinical datasets or alternate models is essential. This would solidify the signatures' roles in tumor initiation and drug resistance. Leveraging publicly available data for this validation would be acceptable. Similar studies performed in melanoma by Arjun Raj's group could be a valuable source for cross-validation and discussion (PMID: 28607484 PMID: 37468627).*

Reviewer2.R5. We appreciate the reviewer's insightful comment and acknowledge the importance of extending our findings to a broader breast cancer context to strengthen their generalisability. A similar comment was raised by Reviewer 1; we refer to **Reviewer1.R1.** for details on gene signature generalisability to other cell line models.

Below, we address the following points: **(1)** large-scale assessment of S1, S2 and S3 signatures in bulk RNA-seq of primary tumours; and **(2)** recurrence of gene expression heterogeneity in a scRNA-Seq cohort of primary tumour samples.

(1) Large-scale assessment of S1, S2 and S3 signatures in bulk RNA-seq of primary tumours. In **Reviewer1.R1**, we evaluated the relevance of the signatures in stratifying basal breast tumours across large cohorts (TCGA and METABRIC) and found that genes in S1 and S2 signatures are more highly expressed in basal tumours, in both datasets. Next, we asked whether the gene signatures were co-expressed in primary tumours. To this aim, we computed cross-gene correlation across both TCGA and METABRIC datasets; the results are reported below. The correlation matrices highlight distinct blocks of mutually correlated genes within the S1 signature, suggesting that genes co-expressed in the S1 population are also co-expressed in primary tumours. We observe co-expression of genes encoding collagen molecules and implicated in the extracellular matrix organisation and other genes involved in the epithelial-to-mesenchymal transition. Despite having been obtained from bulk gene expression information, these blocks contain groups of genes respectively belonging to the same tumour meta-program (S1/EMT-I and S1/EMT-III blocks; see point (2) below and Gavish et al.(DOI: 10.1038/s41586-023-06130-4)), suggesting that they may be part of the same gene expression network.

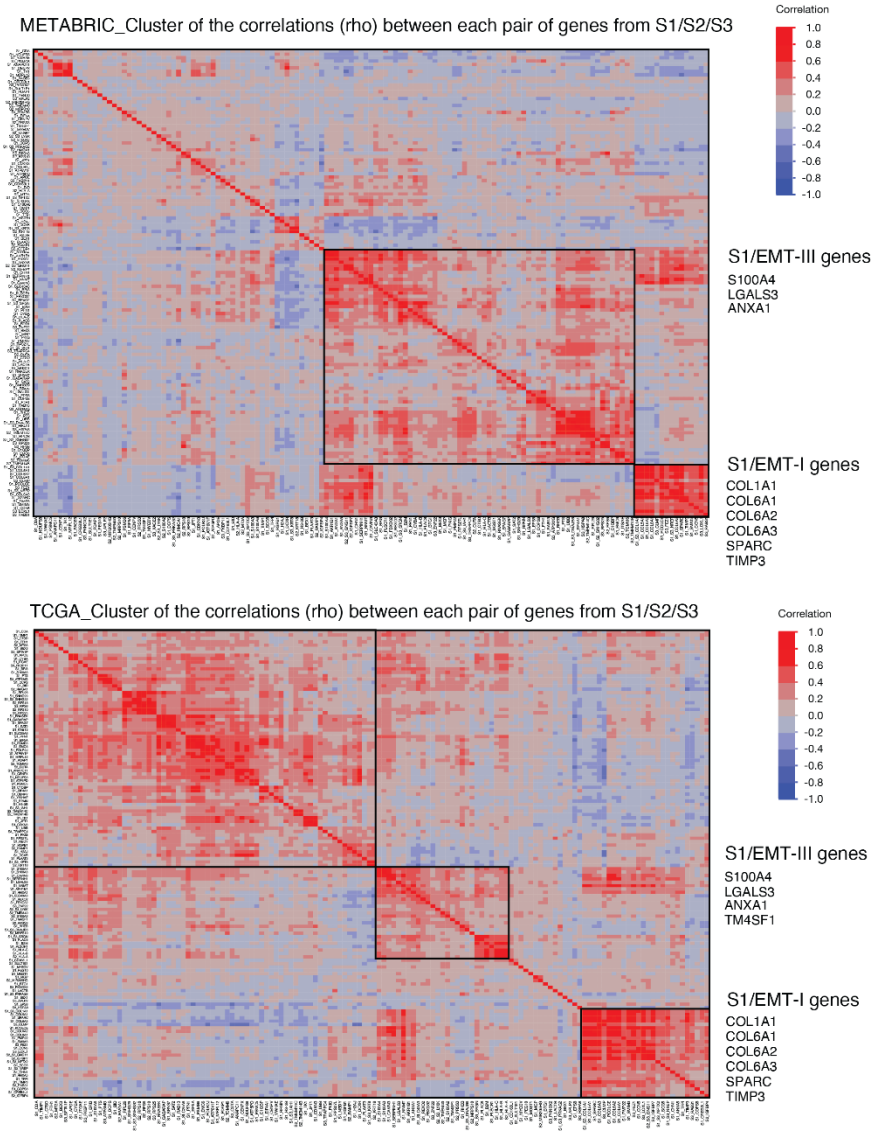

Figure R2.7. Clustering (K-Means) of linear correlations between the expression level (Z-Score, see Methods) of each gene belonging to S1, S2 and S3 gene signatures and METABRIC or TCGA (bottom) datasets.

(2) Recurrence of gene expression heterogeneity in a scRNA-Seq cohort of primary tumour samples. To further corroborate the above results, we evaluated whether the heterogeneity showcased by S1, S2 and S3 in SUM159PT cells is recapitulated within primary tumours, in breast or other tissues. Therefore, we leveraged the Curated Cancer Cell Atlas (3CA, https://www.weizmann.ac.il/sites/3CA/), which contains scRNA-Seq data for over 1000 primary tumour samples from over 70 studies. Gavish et al. obtained a list of meta-programs associated with them, consisting of groups of genes whose expression co-vary within tumours, using non-negative matrix factorisation. Similar approaches have been used previously (e.g., Kinker et al. (DOI: 10.1038/s41588-020-00726-6)) and proved better at capturing recurrent intra-tumour heterogeneity compared to clustering cells into discrete populations. We reasoned that the association of SUM159PT subpopulations to relevant meta-programs obtained from 3CA would be a strong indication for the recurrence of subpopulation signatures in primary tumours. For each meta-program M, we first obtained the top representative 50 genes from Gavish et al.; then, we computed a joint gene expression level (ModuleScore) for each cell; finally, we calculated the area under the curve AUC(S,M) for each subpopulation S (predictor variable = ModuleScore, response variable = the cell belongs to S). The AUC(S,M) values for each subpopulation and for each meta-program are shown below: rows are meta-programs shared across multiple cancer types, as

reported by Gavish et al., and columns are clusters. The heatmap below shows the AUC values for all clusters at T0.

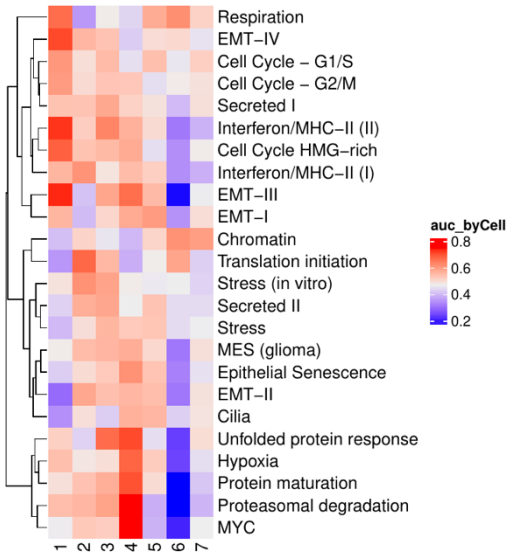

Figure R2.8. Association of gene meta-programs from [Gavish, 2023] with clusters at T0. Only "shared" meta-programs are reported. The entries are the AUC values where the predictor is the aggregate meta-program expression and the response is the membership to each cluster.

The association of meta-programs with cell clusters is non-stochastic: a clear association emerges, for instance, between the first 10 meta-programs and S1 (cluster 1). This suggests that SUM159PT heterogeneity is, at least in part, recapitulated in primary tumours and identifies a common pattern of intra-tumour heterogeneity. Specifically, the “EMT-III” meta-program is enriched in S1 cells, “Interferon/MHC-II (II)” both in S1 and S3 cells, and “Translation initiation” in S2 cells, in agreement with pathway enrichment analysis results (see also **Suppl. Figure 1F**). These findings are recapitulated also in another TNBC cell line (MDA-MB-231 TGL; see **Reviewer1.Q1** details). The figures below show the association of the three meta-programs with S1, S2 and S3 in greater detail: the columns of the heatmaps represent the cells ordered by non-decreasing module score, and the bar plots show the binned cell count for each subpopulation.

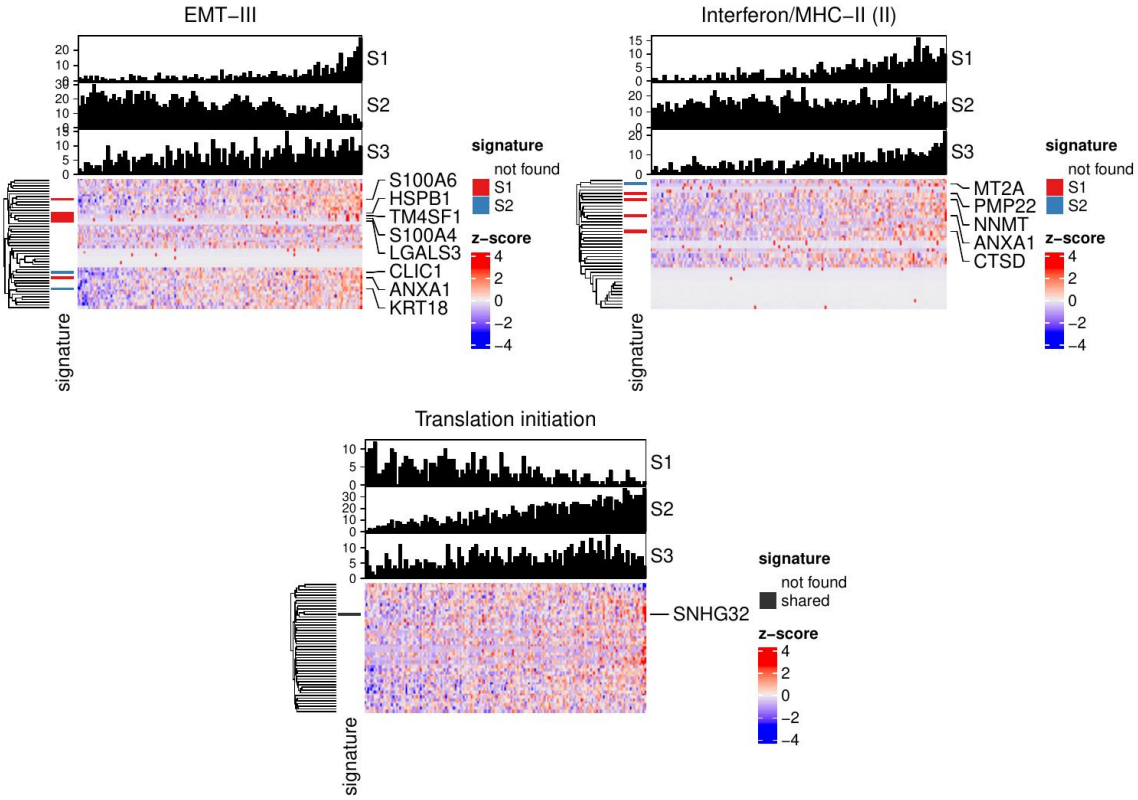

Figure R2.9. Association of SUM159PT cells with three tumor meta-programs from the Curated Cancer Cell Atlas (3CA). The columns of the heatmap are the cells at T0 ordered by non-decreasing module score, computed on the union of the top 50 significant genes of the meta-program, reported in rows; genes shared with the S1 and S2 signatures (S3 was not found) are labelled and marked in colour. The bar plots show the cell count for each subpopulation across 100 bins.

Importantly, “EMT-III” contains genes involved in epithelial-to-mesenchymal transition, includes both epithelial and mesenchymal markers (frequently referred as “hybrid EMT state”), and is reported as a general hallmark by Gavish et al.. In the same paper, it was reported as abundant in several cancer types, notably in breast. The top 50 representative genes for EMT-III include S100A4, TM4SF1, and LGALS3 (marked in red in the figure above), which are also top markers of S1. In addition, we provide further functional evidence that the top 50 S1/EMT-III genes promote tumour aggressiveness in a *in vivo* mouse model of lung cancer, by exploiting the dataset from LaFave et al. (DOI: 10.1016/j.ccell.2020.06.006). Here, the authors leveraged single cell tracking and single cell ATAC-seq to identify the key regulators of epigenetic programs during different steps of transformation. RUNX2 emerged as a hub of the most plastic, pre-metastatic epigenetic module. We found that S1 signature genes, notably its EMT-III component, were ranked among the top scored genes in the RUNX2-driven epigenetic module.

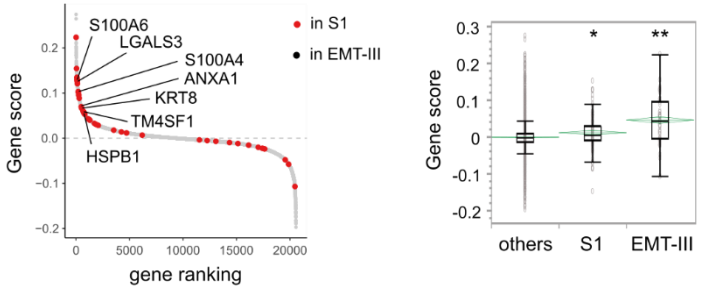

Figure R2.10. Gene signatures in the scATAC-Seq dataset of lung adenocarcinoma from [LaFave 2020]. Left: the *x* axis represents the genes ranked by gene score; the *y* axis is the gene score; S1 signature genes are coloured in red, with those that are also found among the top 50 of the EMT-III meta-program, as defined in [Gavish 2023], labelled. Right: boxplot (with median, upper and lower quartile and whiskers) of the gene scores across different groups. Also shown are individual points (grey circles) and the mean diamonds (green line); * p-value = 0.001, ** p-value < 0.0001, Wilcoxon rank-sum test).

We extensively discussed the recurrence of these genes in cancer and their association with tumour initiation, hybrid EMT and metastatic potential in paragraph "**The baseline programs S1 and S3 predict tumour initiation**".

We added a new panel in **Figure 1**, a new **Suppl. Figure 2**, a new panel in **Suppl. Figure 4, previously S2** and two new **Suppl. Tables 5** and **6.** We added a new section entitled "**SUM159PT transcriptional heterogeneity is recapitulated in primary tumours**" and a new paragraph in section "**The baseline programs S1 and S3 predict tumour initiation**".

Reviewer2.Q6. *While sorting for TM4SF1 seems to enrich for faster and more efficient tumor initiation, sorting for a single marker is risky. Having the "ABCB5+ tumor initiating marker" debate from 2010 in mind, I would have appreciated to see FACS-enrichment for TIC-capacity by more than one marker.*

Reviewer2.R6. We tested both LGALS3 (coding for GALECTIN-3) and TM4SF1, which are the only specific gene expression markers for either S1 or S3. Galectin-3 is partially localized on the cell surface and is a cancer-relevant gene involved in the EMT program (Gavish et al.). However, FAC-sorting using a GALECTIN-3 antibody resulted in a much smaller GALECTIN-3+ cell proportion compared to the TIC population (0.33%, as shown in the graph below; eBioM3/38, PE-conjugated, eBioscience). Therefore, we relied on TM4SF1 expression to enrich for TICs.

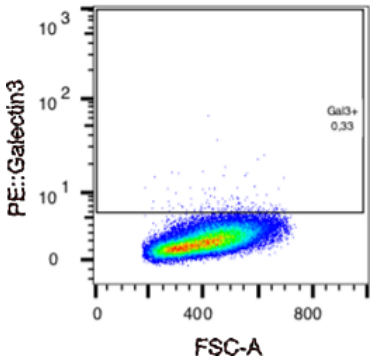

Figure R2.11. FACS plot representing the percentage of GALECTIN-3+ cells in SUM159PT cells. Staining with a monoclonal antibody against Galectin 3 (eBioM3/38 conjugated with PE, eBioscience).

While we agree with the reviewer that sorting for a single marker might be risky (e.g. poor specificity or poor purity), we adopted multiple precautions to avoid biases and confounding factors. Concerning the mentioned ABCB5+ marker, the main point of the debate was a possible dramatic underestimation of the frequency of cancer stem cells in the melanoma models used for the experiment. The TIC frequency that we observed in this work agrees with our previous data on dilution transplantation experiments (range 1:100-1:1000; see Bonetti et al. (DOI: 10.1038/s41388-018-0445-3); Tordonato et al. (DOI: 10.1083/jcb.202009053)). Of note, by transplanting cells 9-days post-sorting (see also **Suppl. Figure 5A**) rather than freshly sorted cells (see also **Reviewer1.Q3**), we removed any possible direct effect of antibody staining (Taussig et al. (DOI: 10.1182/blood-2007-10-118331)). We confirmed that the isolated population (top 5% TM4SF1 fluorescence) shows high expression of many genes of the S1 signatures after 9-day culture compared to the bulk population (see **Reviewer1.R3**). We also confirmed that the antibody was fully specific for TM4SF1 using a knock-down experiment followed by FACS (**Suppl. Figure 5B, previously Suppl. Figure 4B**). Since the distribution of TM4SF1 fluorescence appeared as

a continuum rather than clustering into discrete populations (**Figure 2G**), we applied two gating strategies based on quantiles (top 5% and top10%, **Suppl. Figure 5D)** and measured S1 marker expression by both qPCR and bulk RNA-seq **(Suppl. Figure 6B)** (see also **Reviewer1.R3**).

Importantly, a sorting strategy for TIC based on TM4SF1 enriches for tumour initiation also in human MDA-MB-231 cells, murine 4T1 breast cancer cells, and MMTV-Neu tumours (Gao et al.; Chen et al.).

While acknowledging that future clinical applications may require multiple markers, such as a combination of TM4SF1 and LGALS3, we believe that our approach sufficiently addressed the objectives of this publication, specifically testing the TIC properties of S1 cells, with the implementation of necessary measures and controls.

Reviewer2.Q7. *Even though S2 seems to be a transcriptionally distinct and stable (recurrent) cluster/state it seems to be unrelated with either tumour initiation or drug tolerance. That's surprising as REACTOME enrichment terms include "response to starvation" and many terms related to translation, all known to play roles in drug responses. Any explanation/speculation?*

Reviewer2.R7. A prominent feature of S2 is upregulation of genes associated to tumour progression, such as HMGA1 and MIR205HG. HMGA1 is an oncogene and has been associated to the TNBC subtype [see Mendez et al. (DOI: 10.1158/1078-0432.CCR-18-0517)]. MiR-205 is a basal marker, thus able to promote proliferation of basal progenitor cells [see Ferrari and Gandellini (doi: 10.1038/s41419-020-03192-4). Notably, one of the most highly depleted genes in TM4SF1-high cells is MIR205HG (**Suppl. Table 9**). This suggests that tumour initiation may be promoted by EMT hybrid cells to a higher extent compared to basal progenitors.

Drug tolerance is set up by two distinct clone lineages: lineage 1 is enriched in S3-clones, whereas lineage 2 does not show strong association with any subpopulation at baseline. While the implication of S2 in drug tolerance cannot be excluded, as we observed that S100A2, one of the top markers of S2, is also a marker of lineage 2, both the lack of a clear association between the transcriptional profile of lineage 2 clones before and after treatment and the limited number of replicates (2, T0 and T1) prevent us from drawing any statistically significant conclusion on the role of S2 in drug tolerance.

Finally, it should be noted that we tested only a specific drug (Paclitaxel); more work on other drugs would be needed to determine the full sensitivity profile of S2 cells.

We added a new sentence in section "**SUM159PT exhibits high transcriptional plasticity and comprise three distinct subpopulations: S1, S2 and S3**", with more details on S2 markers HMGA1 and MIR205HG.

Reviewer2.Q8. *The employment of an inducible CRISPR interference strategy targeting regions proximal to COL6A1 and COL6A2, which are notably accessible in S1 cells, led to a reduction in COL6A1 and COL6A2 expression. How does this alteration impact tumor initiation and drug resistance capacities on the SUM159PT model?*

Reviewer2.R8. As discussed in **Reviewer2.R5**, our work aimed at unveiling the transcriptional and epigenetic landscape of tumour initiating cells; we assessed the generalisability of our conclusions by primarily focussing on a recurrent cancer meta-program we detected, centered on hybrid-EMT and Interferon Response. A rigorous functional analysis of the individual elements of the meta-programs relevant for the *in vivo* phenotype should consider the systematic perturbation of each node of the network *in vivo.* For example, this can be obtained by building an sgRNA library and by subsequently performing a drop-out screening upon transplantation in mice. Conversely, testing each gene and each epigenetic region within the identified regulons *in vivo* is impracticable. Specifically, the experiment illustrated in **Figure 4J** was aimed at assessing the role of two specific regions, identified from Multiome data analysis, on gene expression regulation, but was not intended to test their functional implications. We are currently building a sgRNA library containing all the relevant nodes of the GRNs: this will allow us to functionally dissect the network either *in vivo* or in 3D. We plan to describe the results of such a large-scale functional screening in a follow-up study.

Reviewer2.Q9. *Although the study is rich in advanced analytical techniques, its complexity may serve as a barrier to readers who are not well-versed in these specific methods. To enhance reader comprehension, the authors should consider providing concise explanations of specialized analytical techniques used. For instance, in the section "GALILEO links cancer clones with transcriptional*

programs and DNA accessibility states at single-cell resolution", a brief, one-sentence summary of the referenced method (Bravo Gonzalez-Blas et al. 2019) could facilitate a more accessible understanding without necessitating a separate literature review.

Reviewer2.R9. We thank the reviewer for the suggestion and updated the paragraph "**GALILEO links cancer clones with transcriptional programs and DNA accessibility states at single-cell resolution**" with a brief explanation of the referenced method.

Reviewers' Comments:

Reviewer #1:
Remarks to the Author:
The reviewers have addressed the major comments and the revised manuscript is now clearer.

Reviewer #2:
Remarks to the Author:
The authors addressed all my points adequately and improved the manuscript substantially. I hence can recommend its publication.

We thank the reviewers for their positive comments and appreciate that the manuscript was improved thanks to their feedback and suggestions.

REVIEWERS' COMMENTS

Reviewer #1 (Remarks to the Author):

The reviewers have addressed the major comments and the revised manuscript is now clearer.

Reviewer #2 (Remarks to the Author):

The authors addressed all my points adequately and improved the manuscript substantially. I hence can recommend its publication.